Journal of Biomedical Optics

SPIEDigitalLibrary.org/jbo

Diffuse reflectance relations based on diffusion dipole theory for large absorption and reduced scattering

Rolf H. Bremmer
Martin J. C. van Gemert
Dirk J. Faber
Ton G. van Leeuwen
Maurice C. G. Aalders

SPIE

Diffuse reflectance relations based on diffusion dipole theory for large absorption and reduced scattering

Rolf H. Bremmer, Martin J. C. van Gemert, Dirk J. Faber, Ton G. van Leeuwen, and Maurice C. G. Aalders
University of Amsterdam, Academic Medical Center, Department of Biomedical Engineering and Physics, Amsterdam, The Netherlands

Abstract. Diffuse reflectance spectra are used to determine the optical properties of biological samples. In medicine and forensic science, the turbid objects under study often possess large absorption and/or scattering properties. However, data analysis is frequently based on the diffusion approximation to the radiative transfer equation, implying that it is limited to tissues where the reduced scattering coefficient dominates over the absorption coefficient. Nevertheless, up to absorption coefficients of 20 mm^{-1} at reduced scattering coefficients of 1 and 11.5 mm^{-1}, we observed excellent agreement ($r^2 = 0.994$) between reflectance measurements of phantoms and the diffuse reflectance equation proposed by Zonios et al. [*Appl. Opt.* **38**, 6628–6637 (1999)], derived as an approximation to one of the diffusion dipole equations of Farrell et al. [*Med. Phys.* **19**, 879–888 (1992)]. However, two parameters were fitted to all phantom experiments, including strongly absorbing samples, implying that the reflectance equation differs from diffusion theory. Yet, the exact diffusion dipole approximation at high reduced scattering and absorption also showed agreement with the phantom measurements. The mathematical structure of the diffuse reflectance relation used, derived by Zonios et al. [*Appl. Opt.* **38**, 6628–6637 (1999)], explains this observation. In conclusion, diffuse reflectance relations derived as an approximation to the diffusion dipole theory of Farrell et al. can analyze reflectance ratios accurately, even for much larger absorption than reduced scattering coefficients. This allows calibration of fiber-probe set-ups so that the object's diffuse reflectance can be related to its absorption even when large. These findings will greatly expand the application of diffuse reflection spectroscopy. In medicine, it may allow the use of blue/green wavelengths and measurements on whole blood, and in forensic science, it may allow inclusion of objects such as blood stains and cloth at crime scenes. [DOI: 10.1117/1.JBO.18.8.087007]

Keywords: reflectance; spectrometry; diffusion; scattering; absorption; biophotonics; absorption; biomedical optics.

Paper 130292R received May 16, 2013; revised manuscript received Jul. 3, 2013; accepted for publication Jul. 3, 2013; published online Aug. 28, 2013.

1 Introduction

Interpretation of diffuse optical reflectance spectra requires translating the remitted detected light flux from the turbid material into an absorption coefficient by applying photon transport models.[1,2] Although radiative transport theory is the gold standard here,[3] it cannot be used because it lacks analytical solutions that allow general analysis of diffuse reflectances. The diffusion approximation of radiative transport theory[2,4] or empirical relations between reflectance and tissue optical properties[5] is often used as a next best approach. Unlike empirical relations, diffusion theory requires the reduced scattering coefficient, μ_s', to be much larger than the absorption coefficient, μ_a.

Diffuse reflection spectroscopy is applied in several disciplines, e.g., in medicine, in forensic science, in the clothing industry, and in the film animation industry. In this article, we restrict ourselves to medicine and forensic science, where diffuse reflection spectroscopy is used to assess the state of health or disease of patients,[1,2,6] and for example, the age of a blood stain found at crime scenes[7] or the age of bruises when abuse is suspected.[8] In medicine, tissues have μ_s' values in the visible part of the spectrum that vary between 0.5 and 10 mm^{-1}, whereas μ_a of whole blood ranges from 0.1 to 30 mm^{-1}. Consequently, diffusion theory can only be used for infrared wavelengths and/or tissues with small (<1%) blood volume fractions, thus excluding the study of well-perfused organs, or bruises,[8] in addition to whole blood itself.[5,7] In forensic science, large absorption coefficients occur, e.g., in blood stains at crime scenes or colored clothing but also large (reduced) scattering coefficients, e.g., in wool clothing.

An interesting approach to relate the diffuse reflectance to the optical properties is the approximation to diffusion dipole theory[2] by Zonios et al.[1] This model matches our experimental setup and shows applicability for larger values of μ_a, up to $\mu_a \approx 5\ mm^{-1}$, at $\mu_s' \approx 1.7 - 3.2\ mm^{-1}$, hence ratios of μ_a/μ_s' up to 3. Although these findings may already expand the application of diffuse reflection spectroscopy, its use on parenchymatous tissues at visible wavelengths or on strongly absorbing and scattering objects found at crime scenes is still difficult if not impossible.

In this article, therefore, we will further explore the application range of Zonios' model for larger values of the absorption and reduced scattering coefficients. Our approach is to use phantoms with well-defined values for μ_a and μ_s'. We will increase the μ_a from 5 (Refs. 1 and 9) to 20 and the μ_s' from 1.7–3.2 to 11.5 mm^{-1}. Next, we will compare Zonios' approximate equation with exact diffusion dipole theory,[2] which surprisingly allows rationalizing that diffusion theory may remain applicable when absorption is not small compared to reduced scattering. Overall, this approach permits calibration of the experimental set-up of fiber-based probes so that the material optical properties, including small and large μ_a, μ_s', can be related to diffuse reflectance values.

Address all correspondence to: Maurice C. G. Aalders, Academic Medical Center, University of Amsterdam, Department of Biomedical Engineering & Physics, Amsterdam, The Netherlands. Tel: +31205663829; Fax: +31 20 6917233; E-mail: m.c.aalders@amc.uva.nl

2 Methods

2.1 *Diffuse Reflectance Spectroscopy*

Reflectance spectra, $R(\lambda;\mu_a,\mu_s')$, where λ denotes wavelength, were recorded with a noncontact reflectance spectroscopy setup, containing a spectrograph (USB4000; Ocean Optics, Dunedin, Florida), a tungsten-halogen light source (HL-2000; Ocean Optics), and a probe (QR400-7-UV/BX; Ocean Optics), containing six 400-μm core diameter delivery fibers, circularly placed around an identical central collecting fiber. The probe was tilted 13 deg off-normal and fixed at a height of 17 mm above the phantom, implying a measured illumination spot radius of $r_i = 3.1$ mm and a collection radius of the remitted light of $r_c = 2.7$ mm.[5] Reflectance spectra were recorded over the wavelength range of 400 to 900 nm and were smoothed by averaging the data points into bins of 10 pixels, which allowed calculation of a standard deviation that represents noise within the signal. Data analysis was at 611 nm, chosen because the absorbing dye of the phantom has its maximum there.

Phantoms consisted of a mixture of Intralipid 20% (Fresenius, Kabi AG, Bad Homburg, Germany), phosphate buffered saline, and Evans Blue (Sigma Aldrich, St. Louis, MO) as absorber.[5] The refractive index was assumed to be 1.35. The μ_a of each phantom was controlled by varying the concentration of Evans Blue, and the μ_s' was controlled by varying the amount of Intralipid 20%. For high Intralipid concentrations (>8%), μ_s' was corrected for dependent scattering effects.[10] Evans Blue has an absorption of 18 $(\mathrm{g/L})^{-1}\,\mathrm{mm}^{-1}$ at 611 nm. Intralipid 20% has $\mu_s' = 18\ \mathrm{mm}^{-1}$ at 611 nm.[11] Phantoms were constructed with $\mu_a = 0.1, 0.2, 0.4, 1, 2, 3, 5, 10, 20\ \mathrm{mm}^{-1}$, at $\mu_s' = 1$ and $11.5\ \mathrm{mm}^{-1}$, and a separate set was constructed with $\mu_s' = 0.2,\ 0.5,\ 1,\ 2,\ 3.8,\ 5.5,\ 8.9,\ 11.48,\ 12.75,\ 13.6,\ 15.3\ \mathrm{mm}^{-1}$, at $\mu_a = 1$ and $10\ \mathrm{mm}^{-1}$. Additional phantoms were prepared at each μ_s' without Evans Blue added, and utilized as baseline measurements, $R(\mu_a = 0,\mu_s')$. Finally, the reflectance ratio $R(\mu_a,\mu_s')/R(0,\mu_s')$ was calculated.

2.2 *Theory*

Our starting point is Eq. (18) of the diffusion dipole theory approach of Farrell et al.[2] who calculated the diffuse reflectance $R(\mu_a,\mu_s',r)$ as a function of radial distance, r, in response to a pencil beam at $r = 0$ as

$$R(\mu_a,\mu_s',r) = \frac{z_0}{4\pi}\cdot\frac{\mu_s'}{\mu_s'+\mu_a}\cdot\left[\left(\mu_{\mathrm{eff}}+\frac{1}{r_1}\right)\cdot\frac{e^{-\mu_{\mathrm{eff}}r_1}}{r_1^2} + \left(1+\frac{4}{3}A\right)\cdot\left(\mu_{\mathrm{eff}}+\frac{1}{r_2}\right)\cdot\frac{e^{-\mu_{\mathrm{eff}}r_2}}{r_2^2}\right]. \quad (1)$$

$$\mu_{\mathrm{eff}} = \sqrt{3\mu_a(\mu_s'+\mu_a)};\quad z_0 = 1/(\mu_s'+\mu_a);$$
$$r_1 = \sqrt{z_o^2+r^2};\quad r_2 = \sqrt{(1+4A/3)^2\cdot z_o^2+r^2}. \quad (2)$$

Parameter A depends on the refractive index mismatch of the air–tissue boundary and is given by Ref. 2 as

$$A = \frac{2/(1-R_0)-1+|\cos\Theta_c|^3}{1-|\cos\Theta_c|^2}, \quad (3)$$

where Θ_c is the refractive angle and using n as the tissue–air refractive index mismatch, R_0 is given by

$$R_0 = \left(\frac{n-1}{n+1}\right)^2. \quad (4)$$

This means that $A = 3$ for a phantom refractive index of 1.35. The reflectance ratio in response to an irradiation with radius r_i as captured by the collection fiber requires integrating $R(\mu_a,\mu_s')$ and $R(0,\mu_s')$ over the collection spot size with radius r_c, with radial position ρ between $0 \le \rho \le r_c$.[1]

$$\frac{R(\mu_a,\mu_s')}{R(0,\mu_s')} = \frac{\int_0^{r_c}\rho\mathrm{d}\rho\int_0^{2\pi}\mathrm{d}\varphi\int_0^{r_i}R(\mu_a,\mu_s',|\rho-r|)\cdot r\mathrm{d}r}{\int_0^{r_c}\rho\mathrm{d}\rho\int_0^{2\pi}\mathrm{d}\varphi\int_0^{r_i}R(0,\mu_s',|\rho-r|)\cdot r\mathrm{d}r} \quad (5)$$

$$|\rho-r| = \sqrt{\rho^2+r^2-2\rho r\cos\varphi}. \quad (6)$$

Because Eq. (5) cannot be evaluated analytically, a simple but approximate analytical expression for $R(\mu_a,\mu_s')$ was derived by Zonios et al.[1] They replaced the irradiation area with radius r_i by a point source at $r = 0$ and integrated the backscattered light over a circular collection spot with radius r_c as

$$R(\mu_a,\mu_s') = 2\pi\int_0^{r_c}R(\mu_a,\mu_s',\rho)\cdot\rho\mathrm{d}\rho. \quad (7)$$

Using Eqs. (1) and (2) for $R(\mu_a,\mu_s',\rho)$, the result was

$$\frac{R(\mu_a,\mu_s')}{R(0,\mu_s')} = \frac{\frac{1}{2}\cdot\frac{\mu_s'}{\mu_a+\mu_s'}\cdot\left[e^{-\mu_{\mathrm{eff}}z_0}+e^{-(1+4A/3)\mu_{\mathrm{eff}}z_0}-z_0\cdot\frac{e^{-\mu_{\mathrm{eff}}r_1'}}{r_1'}-(1+4A/3)\cdot z_0\cdot\frac{e^{-\mu_{\mathrm{eff}}r_2'}}{r_2'}\right]}{\frac{1}{2}\cdot\left[2-\frac{1}{\mu_s'}\cdot\left(\frac{1}{r_1'}+\frac{(1+4A/3)}{r_2'}\right)\right]}, \quad (8)$$

$$r_1' = \sqrt{(1/\mu_s')^2+r_c^2};$$
$$r_2' = \sqrt{\left(\frac{1+4A/3}{\mu_s'}\right)^2+r_c^2}. \quad (9)$$

We added factor 0.5 in Eq. (8) for completeness, despite canceling out here. This factor was missing in the original Eq. (3) for $R(\mu_a,\mu_s')$ and may have caused the need for the empirical intensity factor 1.66.[1] Further, we did not empirically change z_0 in Eq. (2) into $z_0 = 1/(0.425\mu_a+0.9575\mu_s')$ for $\mu_s' < 10\mu_a$ and $z_0 = 1/\mu_s'$ otherwise, as was done in Ref. 1.

Table 1 Overview of parameters in Eqs. (3) and (4).

	Symbol	Definition	Exact value	Fitted value
Exact theory, Eq. (3)	ρ	Radial position of collection	from 0 to r_i	
	r_i	Illumination spot radius	3.1 mm	
	r_c	Collection spot radius	2.7 mm	
	A	Refractive index parameter	3	
Zonios' model, Eq. (4)	r_c	Collection spot radius	2.7 mm	6.7 ± 0.3 mm
	A	Refractive index parameter	3	2.0 ± 0.4

2.3 *Evaluation*

Exact diffusion dipole theory, Eq. (5), are compared with our phantom measurements by numerical integration of $R(\mu_a, \mu_s', r)$ and $R(0, \mu_s', r)$. Approximate diffusion dipole Eq. (4) is evaluated in two ways: first, with the exact parameters $A = 3$ and $r_c = 2.7$ mm and second, we fitted parameters A, r_c to all phantom reflectance measurements, using a Levenberg–Marquandt fitting algorithm,[12] with error margins represented by 95% confidence intervals. Table 1 summarizes the various parameters for the three situations.

We also evaluate the asymptotic behavior of the reflectance ratio, Eq. (8), for small and large μ_a, μ_s'. We use these results to discuss the method's applicability at larger optical properties.

Table 2 Asymptotic behavior of Eq. (8) for μ_a, $\mu_s' \to 0, \infty$.

$$\lim_{\mu_a \to 0} \frac{R(\mu_s', \mu_a)}{R(\mu_s', 0)} = 1 \tag{2.1}$$

$$\lim_{\mu_a \to \infty} \frac{R(\mu_s', \mu_a)}{R(\mu_s', 0)} = 0 \tag{2.2}$$

$$\lim_{\mu_s' \to 0} \frac{R(\mu_s', \mu_a)}{R(\mu_s', 0)} \to \infty \tag{2.3}$$

$$\lim_{\mu_s' \to \infty} \frac{R(\mu_s', \mu_a)}{R(\mu_s', 0)} = 1 \tag{2.4}$$

$$\frac{R(\mu_s', \mu_a)}{R(\mu_s', 0)} \approx \frac{0.5 \cdot \mu_s'}{\mu_a + \mu_s'} \cdot \left\{ \exp\left(-\sqrt{\frac{3\mu_a}{\mu_a + \mu_s'}} \right) + \exp\left[-\left(1 + \frac{4A}{3} \right) \cdot \sqrt{\frac{3\mu_a}{\mu_a + \mu_s'}} \right] \right\}, \ \mu_a \approx \mu_s' \text{large} \tag{2.5}$$

3 Results

The four limits of Eq. (8), for $\mu_a, \mu_s' \to 0, \infty$, as well as for the case that $\mu_a \approx \mu_s'$ are large, are summarized in Table 2. Except for $\mu_s' \to 0$, these limits give the correct outcomes.

The measured reflectance ratios of the phantoms, as well as the models of Farrell, Eq. (3), and Zonios, Eq. (8), (parameters given in Table 1), are shown in Fig. 1 for varying μ_a at μ_s' are 1 and 11.5 mm^{-1}, and in Fig. 1(b) for varying μ_s' at μ_a are 1 and 10 mm^{-1}. Exact diffusion dipole theory, Eq. (3), has $r^2 = 0.918$, and Zonios' Eq. (4) with exact A, r_c values (3 and 2.7 mm, respectively) has $r^2 = 0.922$, differing from the experimental results, especially for low values of μ_s'. However, Eq. (4) with fitted parameters ($A = 2.0 \pm 0.4$ and $r_c = 6.7 \pm 0.3$ mm) matches much better the phantom measurements, with $r^2 = 0.994$.

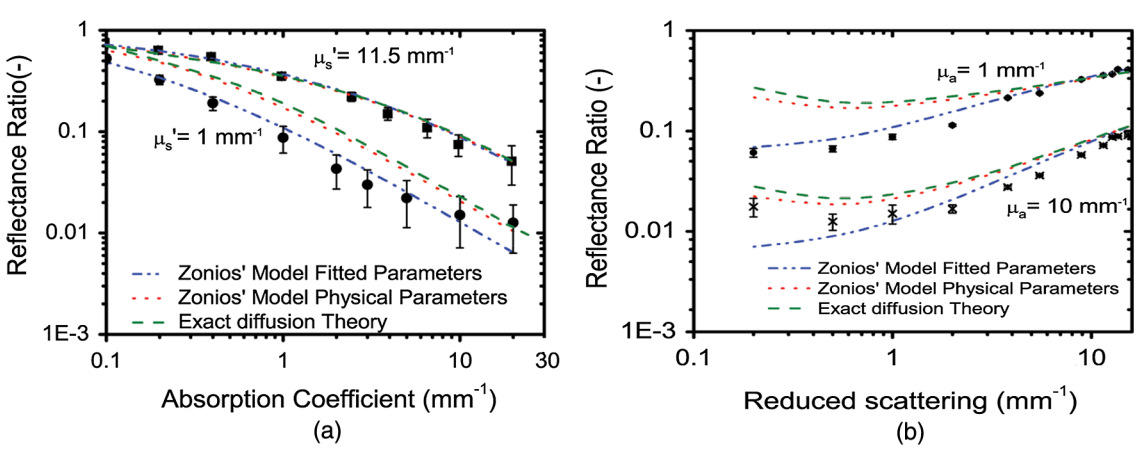

Fig. 1 (a) Reflectance ratio as a function of the absorption coefficient, μ_a, for high (squares) and low (dots) reduced scattering coefficients. Green dashed line: exact diffusion theory, Eq. (3), with $r^2 = 0.918$. Red dotted line: Eq. (8) with exact parameters $A = 3$, $r_c = 2.7$ mm, with $r^2 = 0.922$. Blue dot-dash line: Eq. (8) with fitted parameters $A = 2$, $r_c = 6.7$ mm, $r^2 = 0.994$. (b) Reflectance ratio as a function of the reduced scattering coefficient, μ_s', for high (crosses) and low (dots) absorption.

Finally, the reflectance ratio for large $\mu_a \approx \mu_s'$, Eq. (2.5) in Table 2, gives that $R(\mu_a, \mu_s')/R(0, \mu_s') \to 0.074$. The experimental results [Figs. 1(a) and 1(b)] are 0.087 for $\mu_a = \mu_s' = 1$ mm^{-1} and 0.075 for $\mu_s' = 11.5$ mm^{-1} and $\mu_a = 9.8$ mm^{-1}.

4 Discussion

We have shown that Zonios' approximate diffusion dipole model, Eq. (8), describes the reflectance ratio of phantoms with an r^2 as large as 0.994, even up to $\mu_a/\mu_s' = 20$ at $\mu_s' = 1$ mm^{-1}. This, however, requires fitting parameters A, r_c to all experimental results (Table 1), including those where $\mu_a \gg \mu_s'$. Zonios et al.[1] already reported this for $\mu_a/\mu_s' \approx 1.6 - 3$ but used a different fitting approach (see last paragraph of Sec. 2.2). Venugopalan et al.[9] showed validity for $\mu_a/\mu_s' = 3$, without a fitting procedure. For exact A, r_c parameters and large μ_s', Eqs. (5) and (8) describe the reflectance ratio with an r^2 of around 0.92, even when $\mu_a \approx \mu_s'$. This suggests that diffusion theory may remain applicable beyond its accepted condition of validity to analyze diffuse reflectance spectra, contrary to, e.g., fluence rates (see Fig. 6.2 of Star[4]).

The explanation is based on the following observations. First, Eq. (8) qualitatively describes the morphology of $R(\mu_a, \mu_s')/R(0, \mu_s')$ versus μ_a because the limits for $\mu_a = 0$ and large μ_a, μ_s' are correct. Second, in the numerator of Eq. (8), the last two terms are negligible compared to the first two terms. So, this numerator has two exponentials that include μ_a and one that also includes A. The denominator includes A, r_c. Thus, compared by using exact A, r_c values, fitting the A, r_c to all experiments obviously upgrades Eq. (8) in describing the experiments. In fact, the fitted A is smaller than the exact A (2 versus 3, Table 1). This enhances the importance of the second exponent (e.g., for $\mu_s' = 10$ mm^{-1} and $\mu_a = 1$ mm^{-1}, respectively, 25% versus 12.4% of the first term). Additionally, diffusion theory may remain applicable for higher μ_a because Eq. (8) depends less and less on the actual values of A, r_c if μ_a, μ_s' become larger because the numerator's second term, which includes A, or becomes small relative to the first. It helps that r_c is also relatively large. Hence, Eq. (8), with exact or with fitted parameters, approaches the same outcome when μ_s' and/or μ_a become large.

We acknowledge that Eq. (8) becomes an empirical relation when A, r_c are fitted to all phantom reflectances, as in Zonios' approach.[1] In contrast, Venugopalan's method is based on exact diffusion theory and does not require a fitting procedure,[9] but they limited their experiments to $\mu_a \leq 0.0909$ mm^{-1} and $\mu_s' \leq 0.12$ mm^{-1}, so the applicability for larger absorptions and reduced scattering remains unknown. Nevertheless, compared with empirical relations not based on any underlying theory, where applicability may be limited to a chosen range of μ_a, μ_s' values, Eq. (8) gives correct asymptotes for very small as well as very large μ_a and also for very large μ_s', but not for $\mu_s' \to 0$.

In conclusion, using Eq. (8) with A, r_c parameters fitted to phantom reflectance measurements of widely varying μ_a, μ_s', allows calibration of fiber-probe set-ups so that the diffuse reflectance values can be related to absorption of the materials under study, even when $\mu_a/\mu_s' \gg 1$ and large μ_s'. These findings will greatly expand the application of diffuse reflection spectroscopy. In medicine, it may include blue/green wavelengths in tissues and even whole blood, and in forensic science, it may allow inclusion of strongly absorbing and scattering objects such as blood stains and colored cloth.

References

1. G. Zonios et al., "Diffuse reflectance spectroscopy of human adenomatous colon polyps *in vivo*," *Appl. Opt.* **38**, 6628–6637 (1999).
2. T. J. Farrell, M. S. Patterson, and B. Wilson, "A diffusion theory model of spatially resolved steady-state diffuse reflectance for the noninvasive determination of tissue optical properties in vivo," *Med. Phys.* **19**, 879–888 (1992).
3. A. J. Welch, M. J. C. van Gemert, and W. M. Star, Diffusion Theory of Light Transport in *Optical-Thermal Response of Laser-Irradiated Tissue*, 2nd ed., A. J. Welch and M. J. C. van Gemert, Eds., pp. 145–202, Plenum Press, New York, NY (2011).
4. W. M. Star, Diffusion theory of light transport, Chapter 6, Fig. 6.2 in *Optical-Thermal Response of Laser-Irradiated Tissue*, 2nd ed., A. J. Welch and M. J. C. van Gemert, Eds., Plenum Press, New York, NY (2011).
5. R. H. Bremmer et al., "Non-contact spectroscopic determination of large blood volume fractions in turbid media," *Biomed. Opt. Exp.* **2**(2), 396–407 (2011).
6. N. Bosschaart et al., "Limitations and opportunities of transcutaneous bilirubin measurements," *Paediatrics* **129**(4), 689–694 (2012).
7. G. Edelman, T. G. van Leeuwen, and M. C. Aalders, "Hyperspectral imaging for the age estimation of blood stains at the crime scene," *Forensic Sci. Int.* **223**(1–3), 72–77 (2012).
8. B. Stam et al., "Can color inhomogeneity of bruises be used to establish their age?," *J. Biophoton.* **4**(10), 759–767 (2011).
9. V. Venugopalan, J. S. You, and B. J. Tromberg, "Radiative transport in the diffusion approximation: an extension for highly absorbing media and small source-detector separations," *Phys. Rev.* **58**(2), 2395–2407 (1998).
10. G. Zaccanti, S. Del Bianco, and E. Martelli, "Measurements of optical properties of high density media," *Appl. Opt.* **42**(19), 4023–4030 (2003).
11. H. J. van Staveren et al., "Light scattering of intralipid-10% in the wavelength range of 400 - 1100 nm," *Appl. Opt.* **30**(31), 4507–4514 (1991).
12. K. Levenberg, "A method for the solution of certain problems in least squares," *Q. Appl. Math.* **2**, 164–168 (1944).